Atomic approach to core-level spectroscopy of delocalized systems: Case of ferromagnetic metallic Mn_5Ge_3

L. Sangaletti,[1] G. Drera,[1] E. Magnano,[2] F. Bondino,[2] C. Cepek,[2] A. Sepe,[1] and A. Goldoni[3]
[1]*Dipartimento di Matematica e Fisica, Universitá Cattolica, via dei Musei 41, 25121 Brescia, Italy*
[2]*Laboratorio TASC-INFM, Basovizza, Trieste, Italy*
[3]*Sincrotrone Trieste ScPA, Basovizza, Trieste, Italy*
(Received 11 June 2009; revised manuscript received 6 October 2009; published 4 February 2010)

We present a line-shape analysis based on atomic single configuration Mn $3d^6$ multiplet calculations of core-level and valence-band spectroscopy data from metallic ferromagnetic Mn_5Ge_3. We show that atomic calculations can fit most of the spectral features measured in Mn $2p$-$3d$ x-ray absorption and circular dichroism, in Mn $2p$ and Mn $3s$ core-level photoemission, as well as for the delocalized electrons in valence-band photoemission. This indicates that, in spite of the metallic nature of the compound, atomic effects can play a relevant role to determine the physical properties of the Mn_5Ge_3 system.

DOI: 10.1103/PhysRevB.81.085204 PACS number(s): 79.60.−i, 73.20.−r, 75.50.Pp, 78.70.Dm

I. INTRODUCTION

Atomic effects in photoemission are still attracting a considerable interest, especially in connection with dichroism observed in magnetic systems.[1–6] While photoemission in atomic systems can be in a straightforward way related to theory based on atomic effects, there is an emerging field of investigations where atomic effects are invoked to explain the fine structure observed in condensed phase systems, in particular insulating oxides such as MnO and NiO.[7–9] This approach is based on the multiplet effects that arise from angular momentum coupling between the core hole and the electrons on the outer partially occupied shell, which are localized due to relevant electron-electron correlation effects. Being multiplet splitting a fingerprint of the $3d$ shell occupancy, it has been suggested[3,4] that also charge transfer (CT) effects from the ligand to the metal cation could be accounted for without considering hybridization effects provided that CT is described by using $3d^{n+1}$ atomic configurations.

Apparently, in systems where the outer shell electrons show a remarkable degree of delocalization, multiplet effects in core-level spectra are somewhat blurred. The lack of multiplet features in core-level spectra of the $3d$ transition-metal cation makes a comparison with experiment rather unfeasible, unless one resorts to consider spin-polarized or dichroic photoemission techniques that allow to contrast the contribution of different spin polarizations or majority and minority bands which may result in a fine structure otherwise not observed in unpolarized spectra. An atomic treatment for the Fe case was carried out by Menchero,[10] where by considering an atomic one-particle approach, and neglecting angular momentum coupling between the core hole and the $3d$ electron subsystem, dichroism in photoemission from Fe was calculated. This problem was also treated by the solid many-body approach of Menchero[11–13] as well as by the atomic many-body approach of van der Laan *et al.*[14] for the case of dichroic and spin-polarized photoemission in metallic nickel, by assuming a configuration interaction (CI) among $3d^8$, $3d^9$, and $3d^{10}$ final state configurations, that have been introduced in order to account for satellite features in both core-level and valence-band photoemission.

Atomic effects in photoemission from itinerant Mn-based solid-state compounds have been so far virtually unexplored, in spite of the discovery of magnetic ordering in several Mn-based systems, ranging from the Heusler alloys to Mn silicides. Recent investigations on the Mn-Ge systems have evidenced a ferromagnetic ordering in both single crystals[15,16] and thin-film alloys,[17,18] which make the MnGe system rather interesting for applications in the field of spintronics. The Mn-Ge system was shown to span a wide range of electronic properties from metallic Mn_5Ge_3 single crystals and thin films to semiconducting Mn_xGe_{1-x} binary alloys. Core-level spectroscopies have likewise shown a manifold of results depending on the electronic properties of the system. For this system, only x-ray absorption spectroscopy (XAS) and x-ray magnetic circular dichroism (XMCD) line-shape calculations have been reported so far. While the obvious choice to treat the local electronic structure of semiconducting alloys is that of a localized Mn impurity embedded in a semiconducting matrix, for the case of metallic Mn_5Ge_3 both atomic CI calculations[16] and a bandlike delocalized picture based on density-functional theory (DFT) methods[19] have been proposed to derive the XAS spectral profile.

In the present study we explore to which extent atomic effects in a delocalized system can account for the observed line shape in photoelectron spectroscopy experiments on an ordered, metallic Mn:Ge(111) $(\sqrt{3}\times\sqrt{3})R30°$ reconstructed interface hereafter denoted as Mn_5Ge_3 thin film. Unlike the highly correlated metallic nickel, where several configurations are required to describe the final state of the photoemission process, in the present system we will use an atomic full-multiplet, single configuration approach for an isolated Mn^+ ion to account for the itinerant nature of Mn-related electrons in the conduction band.

II. EXPERIMENTAL AND COMPUTATIONAL DETAILS

The electronic structure of the Mn_5Ge_3 metallic thin film was probed by photoemission spectroscopies and by x-ray absorption spectroscopy across the Mn L edge. The films were obtained by evaporating 14 ML of Mn on the (111) surface of Ge single crystals. Further details on the procedure

TABLE I. Slater integrals G^i and F^i and spin-orbit interaction energies (eV) of the configurations used to calculate the spectral weight in XAS and photoemission experiments.

	F^2_{d-d}	F^4_{d-d}	F^2_{p-d}	G^1_{p-d}	G^2_{p-d}	G^2_{s-d}	ζ_{p-d}	ζ_{d-d}
$3d^5$	9.978	6.206						0.049
$3d^6$	8.797	5.126						0.042
$2p^53d^5$	11.782	7.382	6.788	5.05	2.874		8.023	0.072
$2p^53d^6$	10.777	6.710	6.148	4.498	2.557		8.024	0.064
$2p^53d^7$	9.653	5.963	5.506	3.967	2.255		8.026	0.056
$3s^13d^6$	10.169	6.331				10.753		0.050

to obtain an ordered metallic interface and the experimental conditions are reported in Ref. 20. The calculations of the theoretical spectra are carried out with the Cowan computational codes.[26] All calculations are carried out by assuming that the metallic character of the sample yields a $3d^6$ electron configuration in the outer shell of the Mn ion, i.e., that the overlap between the $3d$ and $4s/4p$ bands increases by one unit the count of $3d$ electrons of atomic Mn. This simple approach has shown to be fruitful for the theoretical analysis of spin-polarized photoemission spectra of Fe determined from *ab initio* wave functions for the ionized states of an isolated $Fe^+(3d^7)$ atomic ion.[21] The Slater integrals (eV) G^i and F^i and the ζ_{p-d} and ζ_{d-d} spin-orbit interaction energies of the configurations used to calculate the spectral weight for x-ray absorption and photoemission spectroscopies are reported in Tables I and II. Following van der Laan and Kirkman,[22] these values have been reduced to about 83%, as is usually done in solids, with the exception of the G^2_{s-d} integral that has been scaled to about 93%.

III. RESULTS

A. XAS and XMCD line shape

In Fig. 1 the XAS spectrum of Mn_5Ge_3 metallic thin film collected at the Mn L edge is shown. Two broad bands at about 642 eV and 653 eV photon energies are detectable, which correspond to the L_{III} and L_{II} edges, respectively. We observe that when the spectrum is compared to that collected from a thinner reacted (i.e., vacuum annealed) 1.3 ML interface,[23] some differences are detected concerning the width of the L_{III} line, which seems to increase with the thickness of the interface. Likewise, while the thinner interfaces show a fine structure, due to possible hybridization of the Mn impurity with Ge orbitals,[23] the weak fine structure features seem to completely disappear in the present thicker (14 ML) film. When atomic calculations are carried out both in the $3d^5$ and $3d^6$ initial state configurations [Figs. 1(b)–1(d)], several differences can be found.

As can be observed, the XAS spectrum of the Mn^{2+} ion in the Hund's rule $^6S_{5/2}$ ground state[26] ($2p^53d^6$ final state) displays a fine structure where five features can be easily identified [A, B, C, D, and E in Fig. 1(d)]. These features well compare, for instance, with those observed for Mn impurities in Cu,[24] where the Mn ion does behave as an isolated impurity in the metallic host matrix. In turn, Mn ions in Mn_5Ge_3 are expected to contribute to delocalized states in the valence-band region and, in this respect, cannot be regarded as isolated ions in the $^6S_{5/2}$ ground initial state. Coming back to calculated spectra, the results for the $2p^63d^6$ configuration [$2p^53d^7$ final state; Figs. 1(b) and 1(c)] are somewhat different. In particular, the L_{II} emission appears to be differently [features G, H, and K in Fig. 1(b)] redistributed with respect to that calculated for the $3d^5$ configuration [D and E in Fig. 1(d)], while the fine structure of the L_{III} line is smoother than that calculated for the $3d^5$ case. The former difference yields a good agreement between the measured L_{II} line shape with the calculated spectrum for the $3d^6$ configuration. This finding has a counterpart in the case of Mn $2p$ core-level photoemission as we will see below. We also observe that the spectrum in Fig. 1(b) for the $3d^6$ configuration was obtained by setting the spin-orbit interaction for the $3d$ electrons to zero, following the approach suggested by Kimura *et al.*[25] This choice is motivated by the delocalized nature of the six $3d$ electrons in the outer shell, which quenches the spin-orbit interaction for $3d$ electrons. In fact, the calculated $3d^6$ XAS spectrum with nonzero spin-orbit coupling on $3d$ electrons [Fig. 1(c)] does not fit well the experimental data.

Important differences between the $3d^5$ and the $3d^6$ cases emerge when the measured XMCD [Fig. 2(a)] is compared to the calculated spectra, as is done in Fig. 2. At first, we observe that the calculated XMCD spectrum for the $3d^6$ configuration [Fig. 2(b)] better fits the experimental data than the spectrum calculated for the $3d^5$ configuration [Fig. 2(c)]. In particular, a better agreement is obtained for the C feature in the experimental XMCD spectrum and for the width of the A spectral feature. A comparison with the experiment allows us to rule out the results obtained by considering the $3d^6$

TABLE II. Slater integrals G^i and F^i and spin-orbit interaction energies (eV) of the $3p^43d^7$ configuration used to account for ND effects in the Mn $3s$ photoemission.

	F^2_{p-p}	F^2_{d-d}	F^4_{d-d}	G^1_{p-d}	G^3_{p-d}	ζ_{p-d}	ζ_{d-d}
$3p^43d^7$	13.172	10.171	6.331	14.028	8.488	0.916	0.050

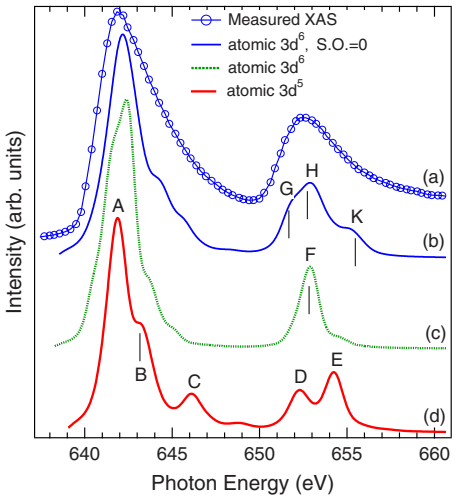

FIG. 1. (Color online) Mn L-edge XAS spectrum of the Mn_5Ge_3 thin film (a) and calculated XAS spectra of the Mn^{2+} ion (d) ($2p^63d^5 \rightarrow 2p^53d^6$), and of the Mn^{1+} ion ($2p^63d^6 \rightarrow 2p^53d^7$) with (c) and without (b) the spin-orbit interaction of $3d$ electrons.

configuration with spin-orbit coupling for the $3d$ shell electrons [Fig. 2(d)]. Also in the XMCD case, the best matching with the experiment [Fig. 2(b)] is obtained by setting the spin-orbit interaction on the $3d$ electron to zero as was done for the Heusler alloys[25] and for the Mn_5Ge_3 single crystals.[16] Finally, it is important to observe that for XMCD the atomic calculation results are in better agreement with experiment than those obtained from density-functional theory models[19] for Mn_5Ge_3 since the latter approach fails to reproduce the experimental B feature [Fig. 2(a)] in the XMCD signal.

B. Photoemission spectra

The analysis of the XAS and XMCD spectra strongly suggests that the atomic $3d^6(Mn^+)$ configuration can be assumed

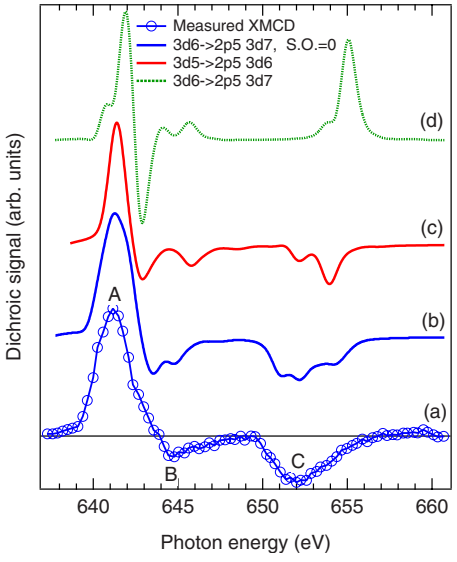

FIG. 2. (Color online) (a) XMCD spectrum measured at the Mn $2p$-$3d$ absorption edge of the Mn_5Ge_3 thin film (T=245 K); calculated XMCD spectrum of the Mn^{2+} ion, $^6S_{5/2}$ ground state (c); Mn^{1+} ion $^5D_4$ ground state with (d) and without (b) spin-orbit coupling for the $3d$ electrons.

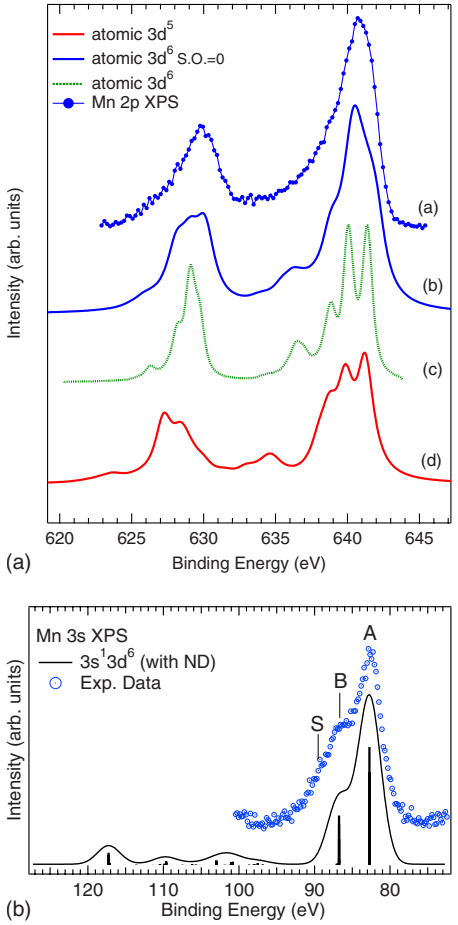

FIG. 3. (Color online) Mn $2p$ and $3s$ core-level photoemission spectra. Top panel: Mn $2p$ XPS spectrum measured with $h\nu$ =960 eV photon energy (a) and calculated spectra based on the [(b), (c)] $3d^6$ and (d) $3d^5$ configurations. Bottom panel: x-ray photoemission ($h\nu$=960 eV) from the Mn $3s$ shallow core levels, Mn_5Ge_3 thin film (dots), and calculated Mn $3s$ spectrum for the $Mn^+(3d^6)$ ion including the near degeneracy effects (thick line).

as the dominant configuration in the ground state of Mn ions. Following this indication we have carried out an analysis of the photoelectron spectra which includes the Mn $2p$ core levels, the Mn $3s$ shallow core levels, and the valence band. Rather interesting is the case of Mn $2p$ core-level photoemission (Fig. 3, top panel). As can be observed, the Mn $2p$ XPS spectrum displays a twofold spin-orbit emission with peaks that are virtually featureless (i.e., no fine structure is detectable). However, an asymmetry on the high binding energy (BE) side of each spin-orbit split component has to be considered in light of the comparison with the calculated spectra. Indeed, this asymmetry is much better reproduced by the calculated spectrum for the $3d^6$ configuration (with ζ_{d-d}=0) than in the $3d^5$ case, where the multiplet features are also much more spread on the BE scale than in the previous case. The spectrum calculated by assuming $\zeta_{d-d} \neq 0$ also does not fit properly the experimental spectrum since it fails to reproduce the width of the Mn $2p_{1/2}$ core line and shows a number of fine structure peaks that are not observed in the Mn $2p_{3/2}$ core line.

We now focus on the Mn 3*s* XPS spectrum in Fig. 3 (bottom panel). The exchange split doublet is clearly detectable, with two peaks (A and B) separated by 4.1 eV. Actually, the separation among the two lines measured in the Mn 3*s* XPS spectrum should be related to the $G^2(3s,3d)$ exchange integral. In particular the measured value is less than 1/2 of that calculated in the atomic case (about 10 eV for Mn^{1+} ions). This is ascribed to near degeneracy (ND) effects that introduce new electronic configurations in the final state of the photoemission process. These configurations are known to be relevant for the low-spin final state contribution and arise from a redistribution of the electrons in the $n=3$ shell among the different (3*s*, 3*p*, and 3*d*) levels. Furthermore, ND accounts for the presence of the spectral features at 20–30 eV toward the higher binding energy. Therefore, following Bagus *et al.*,[27] in the calculation of the final state of the photoemission process also the $3s^23p^43d^{n+1}$ configuration has been included. The addition of this configuration, however, involves only intra-atomic correlations in the final state and the ground state of the system is still described by the single $3s^23p^63d^6$ electronic configuration. The calculated energy separation of the exchange-split doublet is 4.0 eV in good agreement with the experiment. The exchange-related splitting ΔE_{exch} of about 4 eV appears to be lower than those predicted for $3d^6$ electron systems, but we should recall that we are formally dealing with an M^+ ion, i.e., a +1 valence for a $n=6$ electron system. Since the exchange splitting is found to decrease, for a fixed *n*, going from the M^{4+} ion to the M^{+2} ion, a further decrease is expected for the M^{1+} ion, which is indeed what we observed experimentally. This confirms the overall trend predicted for the values of G^2 $(3s,3d)$ and adds an experimental value for the M^{+1} case, which is hardly explored by considering 3*d* transition-metal compounds (simple and mixed oxides, or halides), where the ionization state is usually +2 or larger.

The calculated intensity ratio I_A/I_B between the A and B peaks is 2.51. As expected, this value is different from the one predicted by the rule established by Cox and Orchard[28] for emission form a closed inner subshell, where the intensity (weight) of each multiplet is defined by its total multiplicity, i.e., intensity $\sim(2S^f+1)(2L^f+1)$, where S^f and L^f are the total spin and angular momentum of ionized atom in the final state of the photoemission process. In this case (Mn^{1+}, with ^5D atomic ground state), being $S^f=5/2$ and 3/2 for the high-spin and low-spin contributions, respectively, the expected ratio should be 6/4, i.e., 1.5. The missing spectral weight is, as shown by the calculations, mostly spread in the 90–120 BE range. By including this weight, the expected 6/4 ratio between the high-spin ($S^f=5/2$) and low-spin ($S^f=3/2$) related spectral weights is virtually recovered. As compared to the experiment, the calculated intensity ratio underestimates the experimental value ($I_{A,exp}/I_{B,exp}\sim 1.8$). Furthermore, an asymmetry is observed on the high BE side of peak B. This feature (labeled as S in the bottom panel of Fig. 3) is not fit by the present calculations and could be ascribed to the effects of additional configurations, such as the frustrated Auger configurations involving excitations to the 4*f* shell recently pointed out by Bagus *at al.*[29,30] for the cases of photoemission from Mn and Ni and not included in the present model. These effects may also lead to an intensity redistribution that could increase the calculated intensity of peak B.

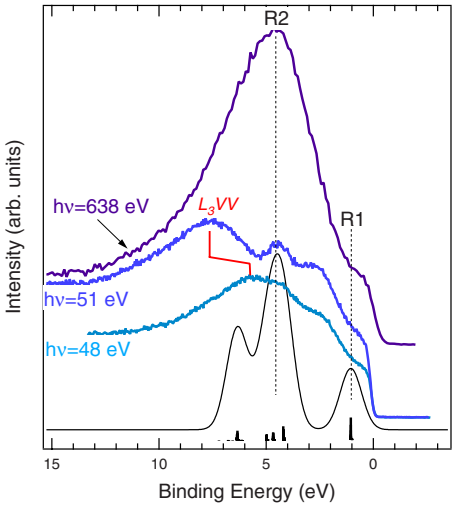

FIG. 4. (Color online) Photoemission spectra from the valence band of Mn_5Ge_3 thin film measured with $h\nu=638$ eV photon energy (Mn 2*p*-3*d* resonant photoemission), as well as with $h\nu=48$ and 51 eV (i.e., across the Mn 3*p*-3*d* resonance), and calculated photoemission spectrum for the $Mn^+(3d^6)$ ion.

Finally, we resort to the resonant valence-band photoemission spectra. In Fig. 4 the valence-band spectrum of Mn_5Ge_3 thin film is shown. This spectrum has been collected at the Mn 2*p*-3*d* absorption threshold in order to maximize the Mn 3*d* spectral weight contribution to the valence band. The spectrum is similar to that reported in Ref. 31, where two spectral features (R1 and R2) were found to be resonantly enhanced. This enhancement is also observed in resonant photoemission across the Mn 3*p*-3*d* absorption threshold, though to a minor extent, as shown in the spectra collected with 51 and 48 eV photon energies, where the resonant enhancement R2 is detectable, along with the normal L_3VV Auger emission. A calculation of the spectral weight in the valence band based on the $3d^6$ initial state (^5D) and a $3d^5$ final state results to be in good agreement with the experimental data. The calculated spectral weight is distributed in the energy range where the R1 and R2 experimental features are detected, and also the intensities qualitatively agree with the observed data. Apparently, this is rather surprising, since the valence-band photoemission probes the electronic states involved in the chemical bonding and, therefore, the more delocalized electronic states. However, since the experimental Mn 3*d* spectral weight has been enhanced by working with photons at the Mn 2*p*-3*d* resonance, the good agreement with the calculations can be interpreted as an indication that atomic effects can be invoked to explain the main spectral features related to the transition-metal atoms in the present metallic system.

IV. DISCUSSION

In our approach solid-state effects are accounted for by setting the spin-orbit interaction for 3*d* electrons to zero and by increasing the 3*d* electron count by one unit. Once we

have made these assumptions we can proceed with an atomic calculation scheme. The point is now to establish which kind of systems can be studied with our approach.

(i) The present atomic scheme is based on the assumption that one single configuration dominates the spectral weight. For example, this is not the case of Ni metal.[14] In turn, iron seems to be more suitable for the application of the present approach, as suggested by the results obtained by Bagus and Mallow on the iron 3*s* core-level photoemission data.[21]

The problem of a proper *d* electron count in metals and metallic compounds is a long-standing question where charge fluctuations are somehow affected by electron-electron interactions and localization effects.[32] In principle, the ground state of an itinerant transition metal is assumed to be described by a broad distribution of different d^n weights which converge toward a single *d* count when electron localization increases because of the effects of the on-site Coulomb interaction *U*. Therefore, in a one-particle model the distribution of the d^n states is given by a binomial distribution that can eventually be modified by electronic correlation effects (see, e.g., Ref. 14 and references therein). Large electronic correlations are supposed to quench charge fluctuations and limit the number of d^n weights. These effects have been invoked to explain the suppression of valence fluctuations observed for the ground state of Mn in MnSi.[33] However, the fact that we are able to describe the Mn spectral weight in Mn_5Ge_3 with a single $3d^6$ configuration does not necessarily imply that on-site Coulomb interaction *U* has become extremely high. Rather, due to the itinerant nature of *d* electrons, also probed by a relevant band dispersion calculated for the bulk Mn_5Ge_3 system and by a strong hybridization between inequivalent Mn ions in the lattice,[19] an increase in the 3*d* count number occurs, quite similar to that observed for the metallic MnSb.[25]

(ii) Furthermore, we can assume that differences in the electronic structure (band structure) may affect the single configuration calculations through a scaling of the HF integrals. This means that the solid-state environment can modify the density of charge (and therefore the energy eigenvalues) related to virtually atomic orbitals when a single atom is embedded into a crystalline environment.

At this point we may try to identify systems that can be treated with the present approach. The system should be metallic and the ground state described by a single $3d^{n+1}$ configuration. Possible candidates are the complex ternary intermetallic Mn-based Heusler alloys[25,34] and the ternary rare-earth intermetallic compounds (RT_2X_2, with R=rare earth, T=transition metal, and X=Si,Ge) such as RNi_2Ge_2,[35] while among binary compounds iron and nickel silicides and germanides could be interesting due their extremely rich phase diagrams which include metallic phases.[36]

In order to discuss the feasibility of our approach to interpret the electron spectroscopy spectra of metallic systems, in the following we will focus on the more simple binary nickel and iron silicides, which have been diffusely studied with high-resolution electron spectroscopies that have produced a large set of spectra for an accurate line-shape analysis. The electronic properties of nickel silicides have been extensively studied and a considerable number of data are available in literature,[37–42] quite often obtained from epitaxially grown Ni layer on silicon single crystals and subsequent annealing.[43–45] A common feature of many core-level and valence-band photoemission data is the presence of satellites a few electron volts below the main line. Bisi *et al.*[41] have pointed out that electronic correlations can play a relevant role in Ni silicides, and therefore we expect that more than one configuration is required to properly describe the photoemission and XAS spectra of these compounds, as was the case of nickel.[14] Indeed, satellites in Ni 2*p* and valence-band photoemission spectra are found in Ni_2Si, NiSi, and $NiSi_2$,[40,41] similar to that observed in pure nickel. When this happens, a CI approach is more suitable to a proper description of photoemission data and makes the present approach unsuitable for the case of Ni silicides.

Iron silicides appear to be somewhat different. For instance two metallic forms of iron silicides are known (the metastable FeSi that crystallizes in a CsCl-type structure and the tetragonal α-$FeSi_2$). Iron core-level photoemission and x-ray absorption data of these compounds are reported in Refs. 46–50. Sirotti *et al.* have carried out a systematic study of synchrotron radiation photoemission and x-ray absorption study of iron silicides[47] and have concluded that Fe core-level satellites have an exchange-interaction origin that cannot be generalized to other ferromagnetic systems such as metallic Ni, where satellites are ascribed to configuration interaction within the highly correlated narrow *d* band of Ni. In light of these results, we believe that iron silicides could be more suitable to apply the single configuration approach than nickel silicide.

V. CONCLUSIONS

In conclusion, we have shown that atomic effects (basically multiplet splitting) can provide a consistent description of photoemission from Mn_5Ge_3 in spite of the metallic character of the system. We believe that this approach can be applied to other systems provided that the metallic character can be treated by adding one electron to the 3*d* electron count to account for possible charge transfer between the 3*d* and the 4*s*/4*p* subshells that are to some extent overlapping (on the energy scale) in the metallic system. By following this idea, we have successfully calculated the XAS and XMCD spectra of Mn in Mn_5Ge_3, the valence-band photoemission, as well as the Mn 2*p* and Mn 3*s* XPS core lines. Using only one configuration for the 3*d* outer shell, but with full accounting for multiplet splitting, most of the experimental features of core-level spectroscopy from a delocalized system can be satisfactorily reproduced, showing to which extent atomic effects can be at work in photoelectron spectroscopies of an itinerant system. Along with the increase in the Mn *d* electron count, setting the spin-orbit ζ_{d-d} interaction to zero resulted to be important to account for the delocalized (metallic) nature of the Mn 3*d* electron system. Furthermore, the XMCD spectrum calculated with the atomic approach is able to reproduce all the main features observed in the experimental data much better than the spectrum calculated on the basis of DFT models.[19]

[1] A. von dem Borne, R. L. Johnson, B. Sonntag, M. Talkenberg, A. Verweyen, Ph. Wernet, J. Schulz, K. Tiedtke, Ch. Gerth, B. Obst, P. Zimmermann, and J. E. Hansen, Phys. Rev. A **62**, 052703 (2000).
[2] R. Müller, J. Schulz, Ph. Wernet, K. Godehusen, M. Martins, B. Sonntag, and P. Zimmermann, Phys. Rev. A **75**, 012718 (2007).
[3] M. Martins, K. Godehusen, T. Richter, P. Wernet, and P. Zimmermann, J. Phys. B **39**, R79 (2006).
[4] M. Martins, K. Godehusen, T. Richter, T. Wolff, and P. Zimmermann, J. Electron Spectrosc. Relat. Phenom. **137-140**, 345 (2004).
[5] B. T. Thole and G. van der Laan, Phys. Rev. B **44**, 12424 (1991).
[6] Kai Starke, *Magnetic Dichroism in Core-Level Photoemission*, Springer Tracts in Modern Physics (Springer, Berlin, 2000).
[7] P. S. Bagus, R. Broer, W. A. de Jong, W. C. Nieuwpoort, F. Parmigiani, and L. Sangaletti, Phys. Rev. Lett. **84**, 2259 (2000).
[8] Ph. Wernet, B. Sonntag, M. Martins, P. Glatzel, B. Obst, and P. Zimmermann, Phys. Rev. A **63**, 050702 (2001).
[9] Kai Godehusen, T. Richter, P. Zimmermann, and M. Martins, Phys. Rev. Lett. **88**, 217601 (2002).
[10] J. G. Menchero, Phys. Rev. B **57**, 993 (1998).
[11] J. G. Menchero, Phys. Rev. B **55**, 5505 (1997).
[12] J. G. Menchero, Phys. Rev. Lett. **76**, 3208 (1996).
[13] J. G. Menchero, Phys. Rev. B **57**, 1001 (1998).
[14] G. van der Laan, S. S. Dhesi, and E. Dudzik, Phys. Rev. B **61**, 12277 (2000).
[15] S. Cho, S. Choi, S. C. Hong, Y. Kim, J. B. Ketterson, B.-J. Kim, Y. C. Kim, and J.-H. Jung, Phys. Rev. B **66**, 033303 (2002).
[16] C. Hirai, H. Sato, A. Kimura, K. Yaji, K. Iori, M. Taniguchi, K. Hiraoka, T. Muro, and A. Tanaka, Physica B **351**, 341 (2004).
[17] Y. D. Park, A. T. Hanbicki, S. C. Erwin, C. S. Hellberg, J. M. Sullivan, J. E. Mattson, T. F. Ambrose, A. Wilson, G. Spanos, and B. T. Jonker, Science **295**, 651 (2002).
[18] P. Gambardella, L. Claude, S. Rusponi, K. J. Franke, H. Brune, J. Raabe, F. Nolting, P. Bencok, A. T. Hanbicki, B. T. Jonker, C. Grazioli, M. Veronese, and C. Carbone, Phys. Rev. B **75**, 125211 (2007).
[19] S. Picozzi, A. Continenza, and A. J. Freeman, Phys. Rev. B **70**, 235205 (2004).
[20] L. Sangaletti, E. Magnano, F. Bondino, C. Cepek, A. Sepe, and A. Goldoni, Phys. Rev. B **75**, 153311 (2007).
[21] P. S. Bagus and J. V. Mallow, Chem. Phys. Lett. **228**, 695 (1994).
[22] G. van der Laan and I. W. Kirkman, J. Phys.: Condens. Matter **4**, 4189 (1992).
[23] A. Verdini, A. Cossaro, L. Floreano, A. Morgante, A. Goldoni, D. Ghidoni, A. Sepe, S. Pagliara, and L. Sangaletti, Surf. Sci. **600**, 4369 (2006).
[24] B. T. Thole, R. D. Cowan, G. A. Sawatzky, J. Fink, and J. C. Fuggle, Phys. Rev. B **31**, 6856 (1985).
[25] A. Kimura, S. Suga, T. Shishidou, S. Imada, T. Muro, S. Y. Park, T. Miyahara, T. Kaneko, and T. Kanomata, Phys. Rev. B **56**, 6021 (1997).
[26] Robert D. Cowan, *The Theory of Atomic Structure and Spectra* (University of California Press, Berkeley, 1981).
[27] P. S. Bagus, A. J. Freeman, and F. Sasaki, Phys. Rev. Lett. **30**, 850 (1973).
[28] See, e.g., C. S. Fadley, *Basic Concepts of X-ray Photoelectron Spectroscopy*, in Electron Spectroscopy: Theory, Techniques, and Applications Vol. 2, edited by C. R. Brundle and A. D. Baker (Academic Press, New York, 1978) and references therein.
[29] P. S. Bagus, R. Broer, and E. S. Ilton, Chem. Phys. Lett. **394**, 150 (2004).
[30] P. S. Bagus, R. Broer, and E. S. Ilton, J. Electron Spectrosc. Relat. Phenom. **165**, 46 (2008).
[31] L. Sangaletti, D. Ghidoni, S. Pagliara, A. Goldoni, A. Morgante, L. Floreano, A. Cossaro, M. C. Mozzati, and C. B. Azzoni, Phys. Rev. B **72**, 035434 (2005).
[32] See, e.g., D. van der Marel and G. A. Sawatzky, Phys. Rev. B **37**, 10674 (1988) and references therein.
[33] F. Carbone, M. Zangrando, A. Brinkman, A. Nicolaou, F. Bondino, E. Magnano, A. A. Nugroho, F. Parmigiani, Th. Jarlborg, and D. van der Marel, Phys. Rev. B **73**, 085114 (2006).
[34] S. Plogmann, T. Schlathölter, J. Braun, M. Neumann, Y. M. Yarmoshenko, M. Yablonskikh, E. I. Shreder, E. Z. Kurmaev, A. Wrona, and A. Slebarski, Phys. Rev. B **60**, 6428 (1999).
[35] J. Park, D. P. Brammeier, C. G. Olson, P. C. Canfield, and D. W. Lynch, Phys. Rev. B **70**, 075105 (2004).
[36] H. Takizawa, K. Uheda, and T. Endo, J. Alloys Compd. **305**, 306 (2000).
[37] A. Franciosi, J. H. Weaver, and F. A. Schmidt, Phys. Rev. B **26**, 546 (1982).
[38] W. Speier, E. v. Leuken, J. C. Fuggle, D. D. Sarma, L. Kumar, B. Dauth, and K. H. J. Buschow, Phys. Rev. B **39**, 6008 (1989).
[39] J. H. Weaver, A. Franciosi, and V. L. Moruzzi, Phys. Rev. B **29**, 3293 (1984).
[40] P. L. Tam and L. Nyborg, Surf. Coat. Technol. **203**, 2886 (2009).
[41] O. Bisi, C. Calandra, U. Del Pennino, P. Sassaroli, and S. Valeri, Phys. Rev. B **30**, 5696 (1984).
[42] I. Jarrige, N. Capron, and P. Jonnard, Phys. Rev. B **79**, 035117 (2009).
[43] T. Nishimura, J. Takeda, Y. Asami, Y. Hoshino, and Y. Kido, Surf. Sci. **588**, 71 (2005).
[44] L. Gregoratti, S. Günther, J. Kovac, M. Marsi, and M. Kiskinova, Appl. Surf. Sci. **144-145**, 255 (1999).
[45] L. Gregoratti, S. Günther, J. Kovac, M. Marsi, R. J. Phaneuf, and M. Kiskinova, Phys. Rev. B **59**, 2018 (1999).
[46] S. Hong, U. Kafader, P. Wetzel, G. Gewinner, and C. Pirri, Phys. Rev. B **51**, 17667 (1995).
[47] F. Sirotti, M. DeSantis, and G. Rossi, Phys. Rev. B **48**, 8299 (1993).
[48] F. Sirotti, M. DeSantis, X. Jin, and G. Rossi, Phys. Rev. B **49**, 11134 (1994).
[49] K. Rührnschopf, D. Borgmann, and G. Wedler, Thin Solid Films **280**, 171 (1996).
[50] B. A. Orlowski, B. J. Kowalski, K. Fronc, R. Zuberek, S. Mickevicius, F. Mirabella, and J. Ghijsen, J. Alloys Compd. **362**, 202 (2004).